RSC Advances

PAPER

View Article Online
View Journal | View Issue

Cite this: *RSC Adv.*, 2015, **5**, 98144

Computational design of a two-photon excited FRET-based ratiometric fluorescent Cu^{2+} probe for living cell imaging†

Dan Wang,[a] Ai-Min Ren,*[a] Jing-Fu Guo,[b] Lu-Yi Zou[a] and Shuang Huang[c]

Received 9th September 2015
Accepted 6th November 2015

DOI: 10.1039/c5ra18393f

www.rsc.org/advances

Though copper ion (Cu^{2+}) is a widely distributed pollutant in the water environment, it plays a vital role in many biological processes. Hence, rapid detection and identification of Cu^{2+} are important. In the past few years, fluorescence sensing has become the golden standard to detect Cu^{2+}, due to its high sensitivity, high selectivity, and useful applications in biology, medicine, environment and chemistry. Thus, researchers have widely concerned with the design and synthesis of Cu^{2+} fluorescent probes. In this study, a novel probe **2a** with high sensitivity and selectivity for detecting Cu^{2+} is designed. It is illustrated that **2a** is a ratiometric fluorescent probe, which recognizes Cu^{2+} by a Förster resonance energy transfer (FRET) mechanism. Meanwhile, the two-photon absorption (TPA) optical properties of **2a** are calculated. The calculated results demonstrate that **2a** possesses a higher energy transfer efficiency upon excitation and a larger TPA peak in the near-infrared region than others. Therefore, it can be inferred that the probe **2a** should be an excellent two-photon (TP) excited FRET-based ratiometric fluorescent probe for Cu^{2+}. The detailed investigations can provide a theoretical basis to synthesize copper-ion-responsive TP FRET-based ratiometric fluorescent reagents, which are powerful tools for the two-photon microscopy (TPM) and biological imaging of Cu^{2+} *in vivo*.

1. Introduction

Transition-metal ions can cause serious health and environmental problems because of their toxicity.[1] As a common transition-metal ion, Cu^{2+} is one of the global widespread pollutants. As the third most abundant transition-metal ion in the human body, Cu^{2+} plays an important role in many biological processes.[2] Some reports suggest that an abnormal accumulation of Cu^{2+} could induce severe neurodegenerative diseases, such as familial amyotrophic lateral sclerosis, Menkes' and Wilson's diseases, Alzheimer's disease and prion disease.[3–5] Hence, rapid detection and identification of Cu^{2+} remain a significant challenge. In the past few years, many techniques have been developed, particularly fluorescence sensing, which has become the golden standard to detect Cu^{2+}, due to its high sensitivity, high selectivity, and useful applications in the chemistry, medicine, environment and biology.[6–8] Thus, it has attracted increasing attention to the design and synthesis of Cu^{2+} fluorescent probes.[9–14]

In general, three basic factors must be taken into account in designing a fluorescent probe: the fluorescence signal, the fluorophore, and the recognition mechanism.[15]

The First is the fluorescence signal. According to the measurement mode, the fluorescence signal can be divided into the fluorescence OFF–ON measurement and the ratiometric measurement. The fluorescence OFF–ON measurement is performed by an increase in the fluorescence intensity without either excitation or emission wavelength shift. It can be influenced by many factors, such as changes of environment around the probe (solvent polarity, pH, temperature, and so forth), collection efficiency of emission, the localization of the probe, the changes of the excitation intensity, and the effective cell thickness in the optical beam, and so on. The ratiometric measurement is the simultaneous record of the fluorescence intensities and their ratio at two wavelengths. It can reduce the influence of environmental factors.[16] Intramolecular charge transfer (ICT) and Förster resonance energy transfer (FRET) are the two most common mechanisms for the design of the ratiometric fluorescent probe.[17] However, some ICT-type ratiometric fluorescent probes have very broad emission band, which make the emission spectra overlap before and after interaction with target analytes. This shortcoming can affect the accuracy of the detection of the fluorescence intensity ratio. On the other hand, FRET has been widely used to construct

[a]*Institute of Theoretical Chemistry, Jilin University, Changchun 130023, People's Republic of China. E-mail: aimin_ren@yahoo.com; Fax: +86 431 88945942; Tel: +86 431 88499567*

[b]*School of Physics, Northeast Normal University, Changchun 130021, People's Republic of China*

[c]*School of Mathematics and Physics, Changzhou University, Changzhou 213164, People's Republic of China*

† Electronic supplementary information (ESI) available. See DOI: 10.1039/c5ra18393f

small-molecule probes and protein- or nucleic acid-based bioprobes. FRET is a non-radiative process; through long-range dipole–dipole interactions an excited dye donor transfers energy to a ground state dye acceptor.[18,19] FRET is considered to be a sensitive and reliable "ruler" over distances of 10–100 Å. It has broad applications in immunoassay, in studying interactions of biological macromolecules, and so on.[20,21] However, it is often seen that the energy acceptor and the energy donor are co-excited due to the overlap of their excitation spectra.[22,23] Meanwhile, scattering light and auto-fluorescence always arise from biomolecules upon the excitation of energy donor. Therefore, new donor–acceptor energy transfer pairs are desired for designing FRET-based probes, especially in bioassays. Recently, two-photon (TP) excitation has received intense attention in biological applications. In this nonlinear optical process, two low-energy photons are simultaneously absorbed to reach the excited state.[24] TP excitable materials can be excited in the near-infrared region (NIR) and show emission in the UV visible region. Under TP excitation with the NIR light, the scattered excitation light and the auto-fluorescence of biomolecules could be eliminated, inducing significantly improved sensitivity. Besides, the NIR light causes much less photodamage and photobleaching.[25,26] The unique features of TP excitation shown above result in its wide use in many fields, notably in microscopic imaging.[27–30] The TP excitable materials are promising energy donors for FRET microscopy, because of the anti-Stokes photoluminescence nature of TP excitation. TP-FRET microscopy has been applied to illuminate protein interactions in tissue and to characterize the intranuclear dimerization of protein molecules in living cells.[31,32] In biological imaging applications, TP-FRET has shown deeper imaging depth, less background, and higher energy transfer efficiency than confocal FRET.[33] So we will focus on the research and design of the TP-FRET ratiometric fluorescent probe in this study.

The second is fluorophore. Similar to other fluorescent dyes, rhodamine dyes are widely used as fluorescent probes owing to their high absorption coefficient and broad fluorescence in the visible region of the electromagnetic spectrum, high fluorescence quantum yield and photostability. Furthermore, rhodamine can construct colorimetric "naked eye" and fluorescence "OFF–ON" probes, owing to the advantages of the open-ring of the spirolactam ring.[34–36] Because of the longer absorption and emission wavelength, the rhodamine fluorophore often acts as the energy acceptor in the FRET systems. In addition, the distance of energy transfer and the extent of the spectral overlap are determined by the target analytes. Considering all above points, rhodamine derivatives should be a good choice for recognition sites and signal switches in FRET systems.

The last one is the recognition mechanism (*i.e.* the interaction or chelation of the analysts with the probes). Like many other transition-metal ions, Cu^{2+} also displays very high affinities for various polyaza ligands. However, the Cu^{2+} can promote the hydrolysis of α-amino acid esters faster than those of other metal ions.[37] A similar molecular recognition/reactivity motif can be incorporated into a fluorophore derivative, which would lead to a fluorescence increase. Hydrazides, hydroxamic acids, and *O*-acyl hydroxylamines are all known as this kind recognition/reactivity motif with resulting enhanced transacylation reactivity.[38] The approach is depicted in Fig. 1. Rhodamine B hydrazide (**3**) is a colorless, non-fluorescent substance. The hydrazide group of compound **3** can provide recognition for the Cu^{2+} by analogy to its reaction with α-amino esters. Upon addition of Cu^{2+} to the colorless solution of hydrazide **3** in acetonitrile, both the pink color and fluorescence characteristic of rhodamine B appear instantly. In acetonitrile Cu^{2+} induces **3** ↔ **5** equilibrium, in much the same way that the proton induces an analogous rhodamine B (**6**) equilibrium in water.[39]

In summary, we focus on investigating a TP-FRET Cu^{2+} ratiometric fluorescent probe with the rhodamine energy acceptor, based on the mechanism of Cu^{2+} promotes the hydrolysis of α-amino acid esters. There has not been any report about TP-FRET Cu^{2+} fluorescent probe so far. Although coumarin–rhodamine-based compounds were rationally designed and synthesized by Lin *et al.* as FRET ratiometric fluorescent chemodosimeters,[12] the energy donor (coumarin) does not have TPA response. In addition, Cho *et al.* first reported the high two-photon fluorescence activity of naphthalene derivatives.[40] According to their research, a new two-photon Cu^{2+} fluorescent probe was reported by Tan' group, using the naphthalene derivative as energy donor and based on through-bond energy transfer (TBET) mechanism.[41] As a proof-of-principle, we design a novel two-photon FRET ratiometric fluorescent probe for Cu^{2+}, in which the rhodamine spirolactam is selected as the energy acceptor for its target-triggered "turn-on" fluorescent signal feature, while the naphthalene derivative is chosen as the FRET donor because of its outstanding TP properties. In this contribution, optical properties of the studied probes, *i.e.* the FRET and the fluorescence OFF–ON effect, are fully rationalized by using density functional theory (DFT) calculations. Our theoretical investigations can provide helpful information for rationally designing the fluorescent probes with high energy transfer efficiency and significant fluorescence switch.

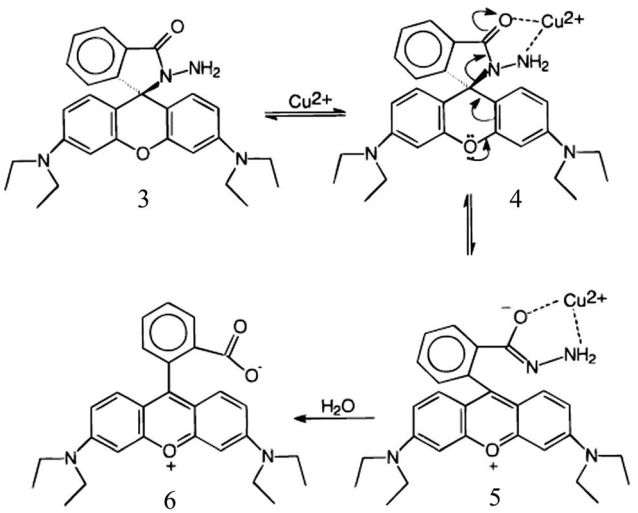

Fig. 1 The recognition mechanism of compound **3** for Cu^{2+}.

2. Computational method

In this work, the geometrical structures of all studied molecules were fully optimized by using density functional theory (DFT) with the 6-31G(d,p) basis set and the M06-2X hybrid functional.[42] In addition, the effect of solvent was taken into account within the self-consistent reaction field (SCRF) theory by using the SMD model.[43] And the frequency calculations of all studied molecules are performed and no imaginary frequency is obtained. On the basis of the optimized structures, the computations of the electronic spectra were carried out by time-dependent density functional theory (TDDFT) using M06-2X* hybrid functional. The M06-2X* method contains 15% HF exchange component, the calculated absorption spectra using this method are confirmed to be in line with the experimental data. On the basis of the ground-state geometries, the M06-2X* (40% HF exchange component) function combined with the 6-31G(d,p) basis set was applied for the first excited state geometry optimization and fluorescence properties in water solvent with the SMD model. All calculations were performed by using the Gaussian 09 program suite.[44] Because all the experimental measurements are carried out in an aqueous environment, therefore, solvation effect is essential. Considering the microsolvation mode, explicit water was added around each of the carbonyl oxygen and the amino group in the calculations, while the implicit solvent effect was considered by SMD.

Moreover, the DALTON program is employed to calculate the TPA properties with 6-31G(d,p) basis set using response theory.[45] The time-dependent DFT/B3LYP method is chosen. From the sum-over-state formulas, the two-photon matrix elements for the resonant absorption of two photons with identical energy are expressed as

$$S_{\alpha\beta} = \sum_s \left[\frac{\langle i|\mu^\alpha|s\rangle\langle s|\mu^\beta|f\rangle}{\omega_{si} - \omega_1} + \frac{\langle i|\mu^\beta|s\rangle\langle s|\mu^\alpha|f\rangle}{\omega_{si} - \omega_2} \right] \quad (1)$$

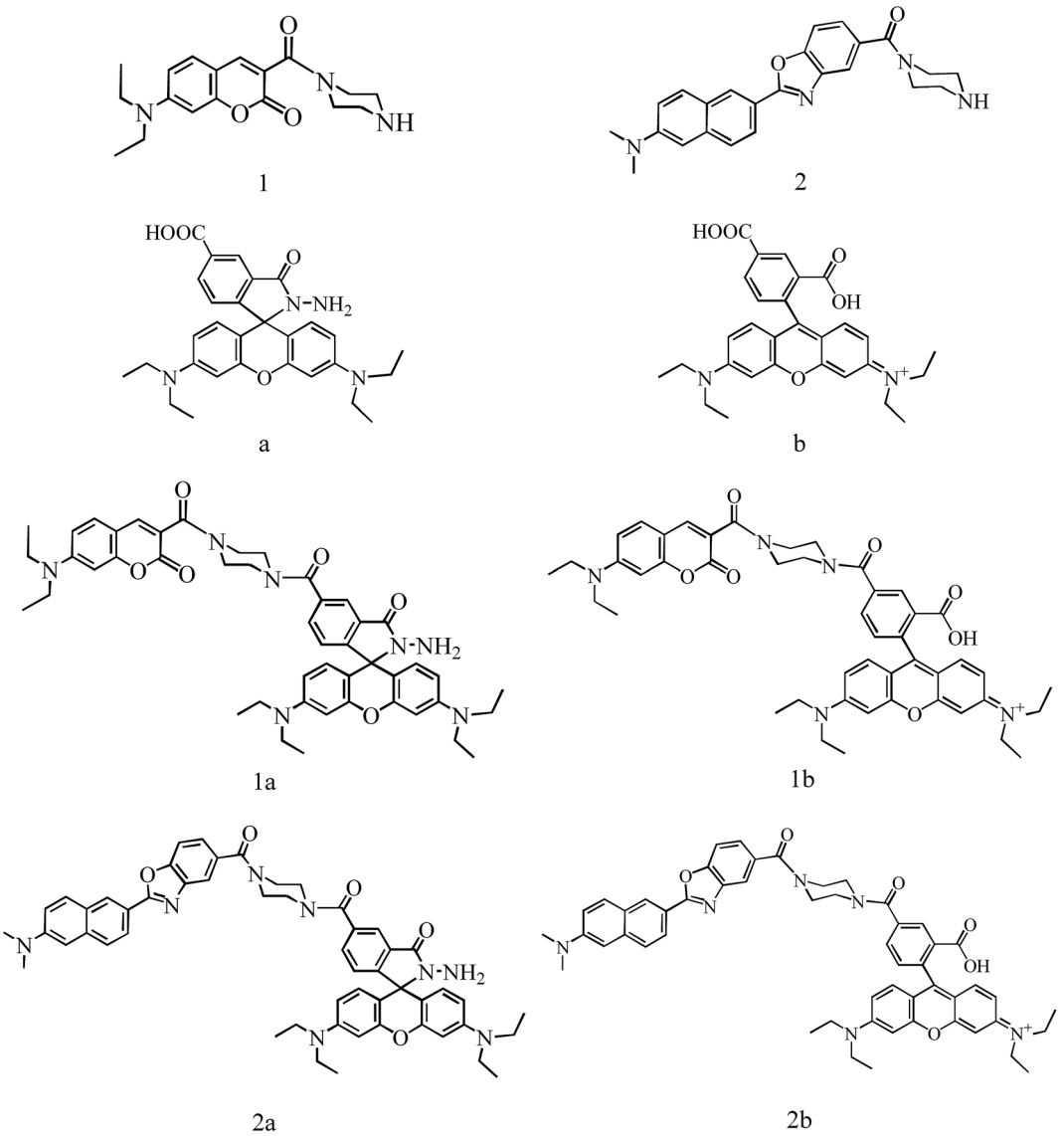

Fig. 2 Chemical structures of studied molecules.

where ω_i is the excitation energy for the intermediate state $|i\rangle$. For molecules in gas phase and solution, the TPA cross section is given by orientational averaging over the two-photon absorption probability:[46]

$$\delta_{tp} = \sum_{\alpha\beta}\left[F \times S_{\alpha\alpha}S^*_{\beta\beta} + G \times S_{\alpha\beta}S^*_{\alpha\beta} + H \times S_{\alpha\beta}S^*_{\beta\alpha}\right] \quad (2)$$

where the coefficients F, H, and G are related to the polarization of the radiation source and the summation goes over the molecular x, y, and z axes. The values of F, H, and G are 2, 2, and 2 for linearly polarized light and −2, 3, and 3 for the circular case.

The TPA cross section directly comparable with experiment is defined as

$$\sigma_{tp} = \frac{4\pi^2 {a_0}^5 \alpha}{15c}\frac{\omega^2 g(\omega)}{\Gamma_f}\delta_{tp} \quad (3)$$

where a_0 is the Bohr radius, c is the speed of light and α is the fine structure constant and $\hbar\omega$ is the photon energy. The lifetime broadening Γ_f of the final state has been assumed to be about 0.1 eV in order to make a sensible comparison with previous results for TPA cross sections of other materials where this value commonly has been used.[47] It should be noticed that such a broadening corresponds to a lifetime of a few fs, which is much shorter than the lifetime of a typical optically excited state. Therefore, it can be believed that such a lifetime broadening should provide a minimal electronic contribution to the TPA cross sections.

3. Results and discussion

3.1 Molecular design and geometrical structures

The structures of the studied molecules in the present work are shown in Fig. 2. Molecules **1** and **2** are the FRET energy donors, while the rhodamine spirolactam (molecule **a**) is selected as the FRET energy acceptor and molecule **b** is the reaction product of molecule **a** and Cu^{2+}. The energy donor **1** and **2** are connected with energy acceptor **a** by the piperazine rigid linker, forming FRET probe molecules **1a** and **2a**, respectively. The rigid linker piperazine moiety can provide a suitable distance between the energy donor and acceptor and avoid the static fluorescence quenching, which can ensure high energy transfer efficiency. The molecule **1a** was reported by Lin's group, as a ratiometric fluorescent chemodosimeter for Cu^{2+}.[12] In molecule **1a**, a hydrazide functional group is the potential reaction site for Cu^{2+}. Notably, the energy donor is far away from the reaction site of Cu^{2+}, which can make the interaction between Cu^{2+} and the reaction site barely affected by the donor. In molecule **2a**, molecule **2** is used as the FRET donor for its outstanding TP response; meanwhile, it retains the advantages of the above design.

Optimized ground state molecular geometries are listed in Fig. S1.† In all molecular structures, the energy donors are planar structure, in the rhodamine acceptor of both ring-closed form and ring-opened form, the benzene and the xanthene were vertical. In FRET molecules, the energy donor and the benzene of rhodamine acceptor tend to be parallel, which is beneficial to FRET process. On the basis of molecular equilibrium geometries, the optical properties of studied molecules are calculated and discussed in the following sections.

3.2 One-photon absorption (OPA) spectra and electronic structures

The OPA process is closely related to the fluorescence and two-photon absorption process, so calculations and analysis of the OPA properties are necessary. The OPA properties of the studied molecules have been calculated by the TDDFT/M06-2X*/6-31G(d,p) method. The visible absorption spectra of the studied molecules are presented in Fig. 3–6. The detailed OPA wavelengths (λ^O_{max}), the oscillator strengths (f^O), the transition nature and the reported experimental data are all listed in Table S1.†

It can be seen from Fig. 3–6, the donors **1** and **2** have absorption peaks in the range of 420–450 nm. The ring-closed form acceptor **a** has no obvious absorption in the visible light range, and the ring-opened form acceptor **b** has a strong absorption at 540 nm. When the acceptor and the donor have been connected by the piperazine linker, the electronic

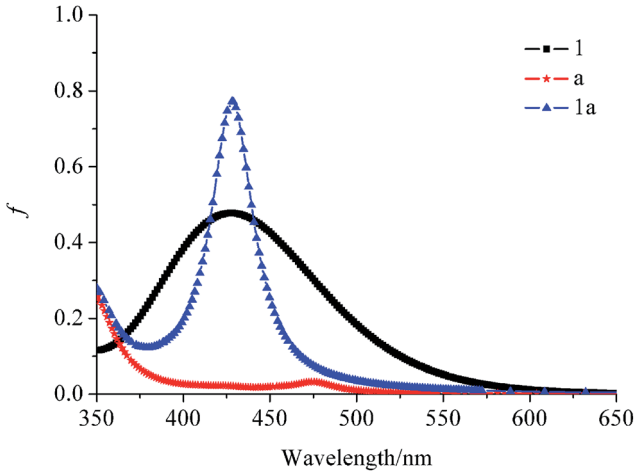

Fig. 3 The OPA spectra of **1**, **a** and **1a**.

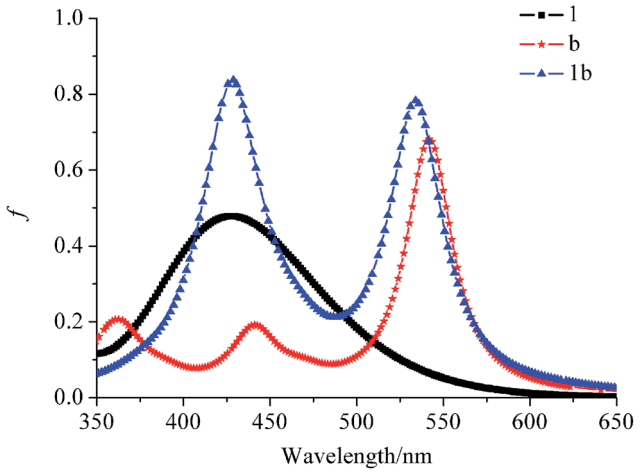

Fig. 4 The OPA spectra of **1**, **b** and **1b**.

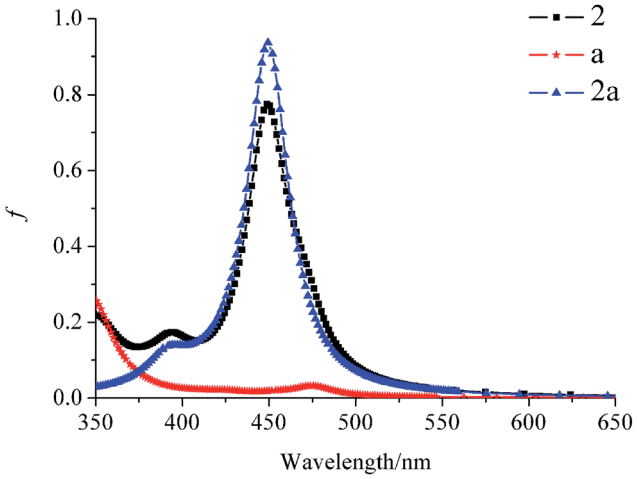

Fig. 5 The OPA spectra of **2**, **a** and **2a**.

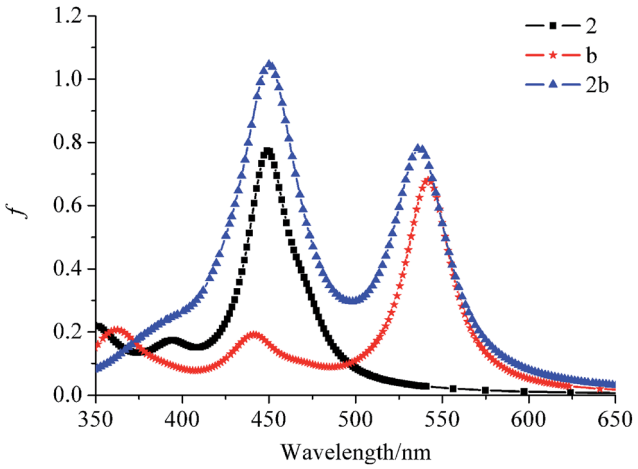

Fig. 6 The OPA spectra of **2**, **b** and **2b**.

absorption spectra of probe molecules are a linear superimposition of donor and acceptor, indicating that it is absent of strong ground-state electronic interaction between the two dyes in probe molecule. In UV-visible light range, the probe molecules **1a** and **2a** just show the absorption of the energy donor, due to there is no absorption of the energy acceptor **a**. Both molecules **1b** and **2b** simultaneously show the absorption peaks of the energy donor and acceptor.

To better explain this spectral phenomenon, the natural transition orbitals (NTO) were calculated at the same level. Natural transition orbital pairs corresponding to each OPA peak are shown in Fig. 7. As shown in Fig. 3, 7 and Table S1,† the donor **1** has an absorption peak at 420 nm, the corresponding transition is $S_0 \rightarrow S_2$, and the corresponding natural transition orbital pair is shown in Fig. 7. From Fig. 7, it can be observed that the absorption peak of molecule **1a** is contributed by energy donor; the long-wavelength absorption peak of molecule **1b** is contributed by energy acceptor and the short-wavelength absorption peak is contributed by energy donor, respectively; the similar changing trends occur in molecules **2a** and **2b**,

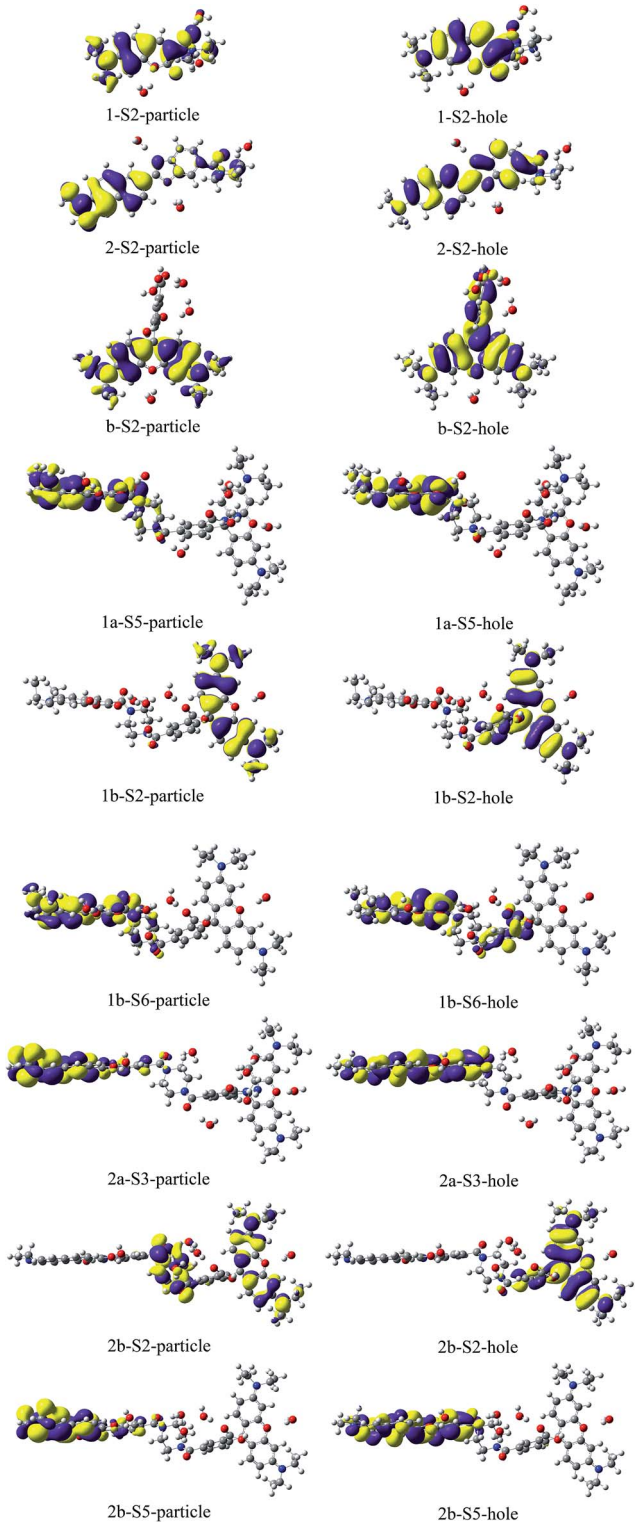

Fig. 7 The dominant natural transition orbital pairs of the OPA corresponding excited singlet states of all studied molecules. For each state, the "particle" is on the left, the "hole" on the right.

revealing that there is no strong ground-state electronic interaction between the energy donor and acceptor, the energy donor and acceptor can be individually excited at their characteristic absorption peaks, which is conductive to FRET process.

3.3 Fluorescence property and identification of Cu^{2+}

For the ratiometric fluorescent probes, fluorescence can be achieved when the excited dyes go back to the ground state, meanwhile, the changes of fluorescence signal can be token for the detection and identification of targets. Thus, the first excited state geometrical optimization and fluorescence properties were performed by the M06-2X* (40% HF exchange component) functional with the 6-31G(d,p) basis set in water solvent. The first excited state optimized geometries are shown in Fig. S2.† Compared with the ground state geometries, the first excited state geometries have little changes. At the same time, the calculated fluorescence emission spectra are shown in Fig. 8–11, the detailed fluorescence emission wavelength (λ^{flu}), oscillator strength (f^F), and transitional nature are shown in Table S2.† The values in Table S2† show that the calculated results agree well with the experimental data. From Fig. 8–11 and Table S2,† donor **1** has an emission peak at 465 nm, and donor **2** has a longer emission wavelength at 500 nm, which is closer to the absorption peak of energy acceptor, indicating that there is greater spectral overlap. Although there is a dark state at 471.94 nm, the acceptor **a** in closed ring form is no fluorescence (calculated f^F is almost zero), which is also confirmed by experimental data.[39,48] The open ring form acceptor **b** has an emission peak at 630 nm. The probe molecules **1a** and **2a** just show the emission of the energy donors, respectively, which can be ascribed to the two factors: the first is that the excitation energy can't excite the acceptor **a** upon excitation at 420 nm or 450 nm (the energy donor maximal absorption); the second is the emission energy of the energy donor **1** and **2** is not enough to excite **a**, so there is no FRET. For the **1b** and **2b**, only the emission peaks of energy acceptors are observed. When the energy donor is excited, the FRET process occurs and the fluorescence of the acceptor is captured. Upon excitation at the characteristic absorption peak of the energy donor, the **1a** and **2a** molecules are catalytically hydrolyzed by Cu^{2+} to form **1b** and **2b** molecules, the emission spectra are changed from energy donor emission into energy acceptor emission. The change of the fluorescence signal indicates the realization for selective recognition of Cu^{2+}. To more clearly understand the

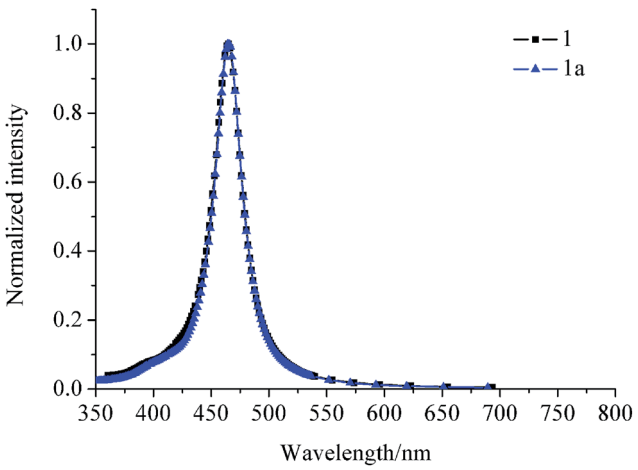

Fig. 8 The normalized emission spectra of **1** and **1a**.

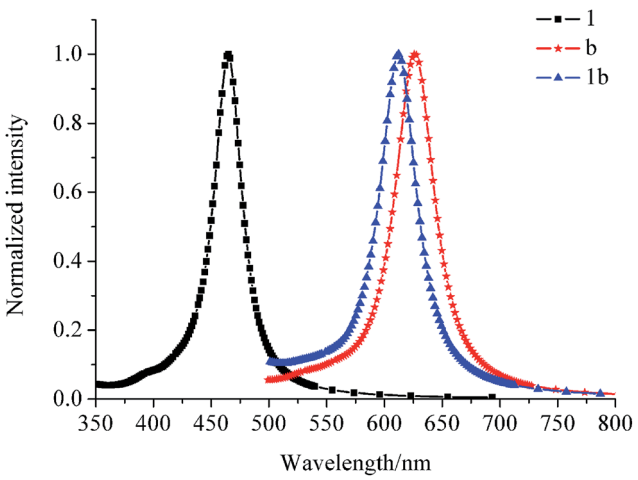

Fig. 9 The normalized emission spectra of **1**, **b** and **1b**.

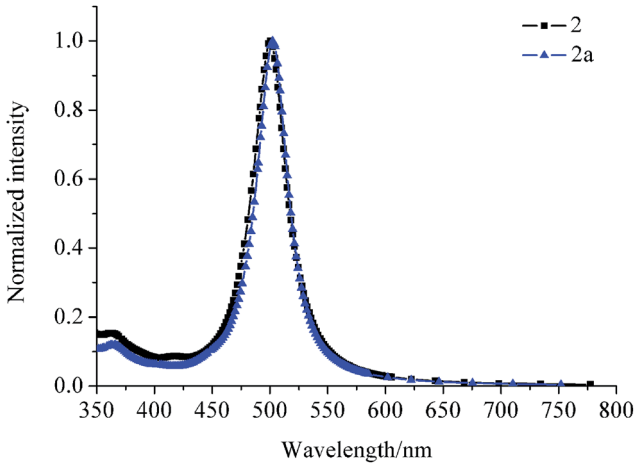

Fig. 10 The normalized emission spectra of **2** and **2a**.

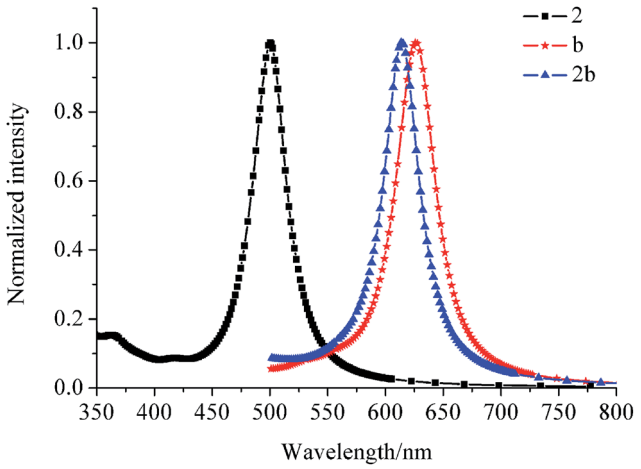

Fig. 11 The normalized emission spectra of **2**, **b** and **2b**.

fluorescence spectra phenomenon, the frontier molecular orbitals related to the main transitions in the emission process are drawn, illustrated in Fig. 12. From Fig. 12, it can be observed that the transitions of the molecule **1a** and **2a** are contributed by the orbits located on the energy donor, so they show the same emission with the energy donor; the emission features of **1b** and **2b** are dominated by the orbits which locate on the energy acceptor part, resulting in the appearance of characteristic emission of energy acceptors. For excited states, the frontier molecular orbitals related to the fluorescence emission process are entirely localized on the energy donor or energy acceptor, which ensures the generation of separate characteristic emission peaks. It is in favor of the identification of Cu^{2+}.

3.4 FRET efficiency prediction

For FRET system, the energy transfer efficiency is very important, which directly determines the sensitivity of the probe molecule. For FRET systems based on organic fluorophores, generally, there is the efficient spectral overlap between the donor emission and the acceptor absorption. The FRET efficiency (Φ_{ET}) is given by eqn (4):[19]

$$\Phi_{ET} = R_0^6/(R_0^6 + R^6) \quad (4)$$

where R_0 is the Förster critical distance at which the transfer efficiency $\Phi_{ET} = 50\%$; R is the distance between the energy donor and acceptor. The Förster distance R_0 can be calculated by simplified eqn (5),

$$R_0 = 0.211[k^2 n^{-4} \Phi_D J_{DA}]^{1/6} \quad (5)$$

where k is the average squared orientational part of a dipole–dipole interaction (it is typically assumed $k^2 = 2/3$ for common organic fluorophores provided that both partners are freely moveable and thus randomly oriented), n is the refractive index, Φ_D is the donor quantum yield, and J_{DA} denotes the degree of spectral overlap between the donor emission and the acceptor absorption, which is given by eqn (6),

$$J_{DA} = \int_0^\infty I_D(\lambda)\varepsilon_A(\lambda)\lambda^4 d\lambda \quad (6)$$

where $I_D(\lambda)$ is normalized fluorescence emission spectrum of the donor, $\varepsilon_A(\lambda)$ is the molar absorption coefficient of the acceptor, and λ is the wavelength.

The spectral overlap between the donor emission and the acceptor absorption of molecules **1b** and **2b** are shown in Fig. S3 and S4.† Based on the above equations, the J_{DA}, R_0 and Φ_{ET} for the FRET-based molecules **1b** and **2b** are shown in Table 1. As shown in Table 1, the Φ_{ET} values of **1b** and **2b** nearly reach 100%; the J_{DA} of **2b** is larger than that of **1b**, meaning **2b** molecule is more advantageous to FRET process; the R_0 of **2b** is larger, which makes the choice of the rigid linker more flexible and broader. So the molecule **2b** is a more excellent FRET-based molecule.

For the FRET process, it is necessary to predict an appropriate alignment of the absorption and emission transition moments and their vectors, as well as a high Φ_D, a substantial J_{DA} and the proximity R. Ideally, the absorption and emission transition dipoles have large vectors in the same direction, which is beneficial to the long-range dipole–dipole interaction. In this paper, we set the X-axis on the short axis of the xanthene structure of rhodamine, the Y-axis on the long axis direction of xanthene structure, and the Z-axis perpendicular to the plane of xanthene, shown in Fig. 13. After fixation of coordinate direction, transition dipole vectors corresponding to both the

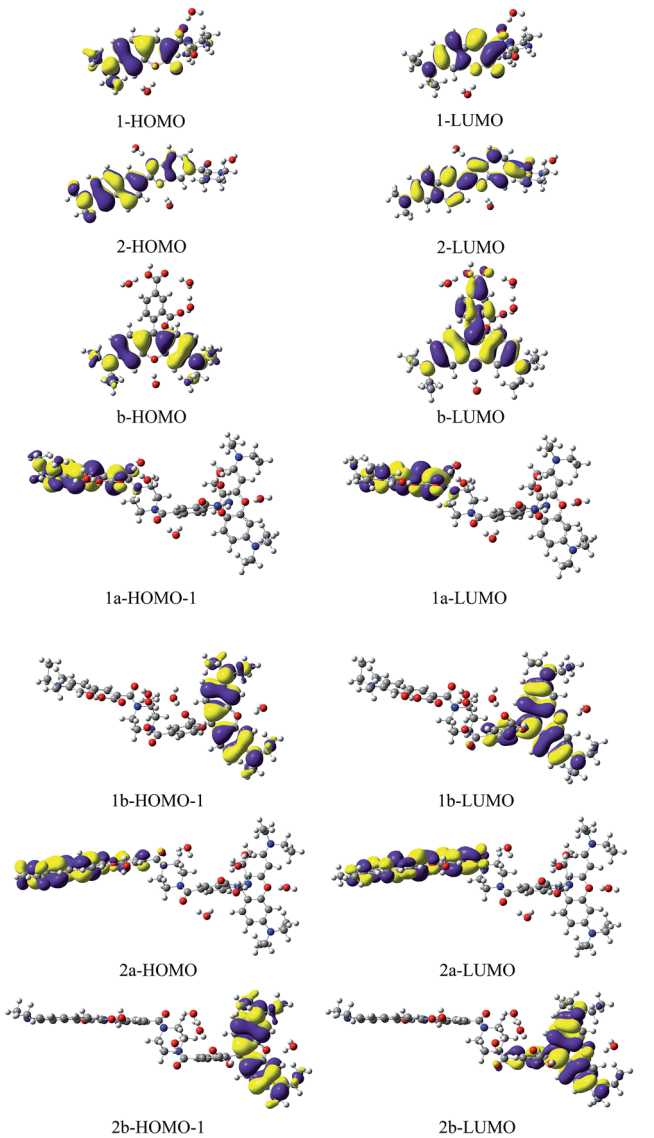

Fig. 12 Contour surfaces of the frontier orbitals relevant to emission for studied molecule.

Table 1 Calculation data of energy transfer for compounds **1b** and **2b**

	J_{DA}/M^{-1} cm^{-1} nm^4	k^2	n	Φ_D	R_0/Å	R Å^{-1}	Φ_{ET} (%)
1b	6.21×10^{14}	2/3	1.33	0.32[a]	39.39	10.33	99.97
	3.62×10^{14}[a]				36.00[a]	11.03[a]	99.9[a]
2b	1.62×10^{15}	2/3	1.33	0.98[b]	55.70	10.83	99.99

[a] Is from ref. 12. [b] Is from ref. 49.

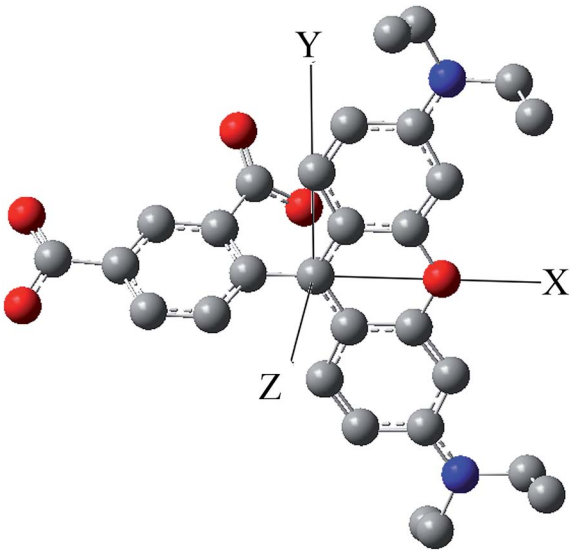

Fig. 13 Schematic of coordinate direction.

emission of energy donor **1**, **2** and the absorption of energy acceptor **b** are calculated, shown in Table 2. From the data of Table 2, the acceptor **b** has a large transition moment vector in the *Y* direction. For donor molecules **1** and **2**, there are large transition moment vectors in the *Y* direction to make sure the FRET can occur, although the maximum transition moment vector is in the *X* direction. What's more, transition moment vector of **2** is bigger than that of **1** in the *Y* direction, demonstrating that molecule **2** is a more excellent donor to rhodamine acceptor.

3.5 Two-photon absorption (TPA) properties

The results and analysis of the OPA process, fluorescence process and FRET efficiency have demonstrated that the probe molecules **1a** and **2a** can effectively identify Cu^{2+} through FRET process. Importantly, recent model studies have confirmed that two-photon probes can be designed using the same strategies with one-photon probe, with the exception that an efficient two-photon fluorophore should be used. Compared with confocal FRET, TP-FRET has shown deeper imaging depth, higher energy transfer efficiency, less background and photobleaching, and less photodamage to biological samples. What's more, the donor **2** is reported as a good TP fluorophore.[40,49] So the TPA properties of the designed molecules are theoretically discussed. The DALTON program has been used to investigate the TP properties of organic molecules. The results obtained from DALTON program are reliable for qualitative description of the molecular TPA features, although sometimes the calculations are persecuted by quantitative problems.[50,51] The TPA properties of the studied molecules have been calculated by using the B3LYP hybrid functional and 6-31G(d,p) basis set, employing a quadratic response function approach, which is implemented in the DALTON program. In the range of 700–800 nm, the number of TPA final states, the excitation energy (E), the maximum TPA wavelength (λ^{T}_{max}), the maximum TPA cross-section (δ^{T}_{max}) and corresponding transition dipole moment (M) are all summarized in Table 3. The detailed values are listed in Table S3.†

Table 2 The transition moments of the donor emission and acceptor absorption and their separation vector

			Transition electric dipole moments/a.u.		
	λ_{max}/nm	f	X	Y	Z
1-Emission	465.60	1.0946	−3.4621	−2.1020	−0.6712
2-Emission	501.08	1.8031	−4.7542	−2.3613	−1.2299
b-Absorption	541.84	0.6741	−0.0243	3.4569	0.1932

Table 3 TPA properties of studied molecules

Molecules	Final state	E/eV	λ^{T}_{max}/nm	δ^{T}_{max}/GM	M/D	EXP
1	2	3.55	698.5	12.5	6.13	
2	1	3.41	**727.2**	**144.5**	8.34	153 GM/780 nm (ref. 49)
a	1	3.35	740.2	37.7	1.74	
b	2	3.17	782.2	63.4	1.16	
1a	3	3.53	702.5	15.2	7.79	
1b	11	3.19	777.3	48.3	1.46	
	15	3.49	710.5	38.0	7.79	
2a	2	3.37	**735.8**	**227.5**	8.94	
2b	17	3.17	782.2	59.9	1.82	
	18	3.25	**763.0**	**359.9**	8.33	

From the data of Table 3, donor **1**, acceptor **a**, probe **1a** and molecule **1b** do not have significant TP response in the NIR (δ^{T}_{max} < 100 GM). The donor **2** has the maximum TPA peak at 727 nm; its δ^{T}_{max} is 144.5 GM. The **2a** molecule has the maximum TPA peak at 735.8 nm, which is contributed by the energy donor **2**. The molecule **2b** simultaneously shows two-photon responses of the energy donor **2** and acceptor **b**. The TP response contributed by energy donor **2** is more obvious; δ^{T}_{max} is 359.9 GM. As we known, the transition dipole moment (M) is one of the important variables for the TPA response. The corresponding transition dipole moments (M) are calculated and shown in Table 3. It is found that the larger M values lead to larger TPA cross-sections for molecules, suggesting the magnitudes of M dominate TPA cross-sections for **2**, **2a** and **2b**. However, it is important to note that the value of M is not the only determinant of the TPA response.

For probe **2a**, using 735.8 nm laser as the TP excitation light, the probe is excited and the fluorescence emitted from the energy donor is observed, because of no FRET; when the Cu^{2+} is present, **2b** molecule produces and the FRET process occurs, the fluorescence of acceptor can be observed. In a word, when the probe **2a** is excited by TP, the detection of Cu^{2+} is still efficiently achieved, and avoids from the photodamage to biological samples.

4. Conclusions

In this work, a new two-photon ratiometric fluorescent probe **2a** for the detection of copper ion (Cu^{2+}) is constructed and estimated. Consequently, we confirmed that **2a** is dominated by

Förster resonance energy transfer (FRET) mechanism for fluorescence imaging. The geometrical structures, one-photon absorption (OPA) properties, fluorescence properties, electronic structures, FRET process and the two-photon absorption (TPA) properties of the probe molecules were studied by theoretical chemistry computations. The new probe **2a** has OPA peak at 450 nm and fluorescence emission at 500 nm. With addition of Cu^{2+} to probe **2a**, **2a** is catalytically hydrolyzed by Cu^{2+}, the hydrazide ring is opened to form **2b** molecule, and its emission spectrum is shifted from 500 nm to 630 nm, thus the obvious changes in the fluorescence signal is conductive to the recognition of Cu^{2+}. The analysis of the FRET efficiency illustrates that **2a** has a higher energy transfer efficiency. Therefore, the probe **2a** is a more effective FRET-based ratiometric fluorescent probe for detecting Cu^{2+}. Significantly, the novel probe molecule **2a** has a large TPA peak in the near-infrared light region. The sensing mechanism typically utilized in the one-photon probe is also compliant in a two-photon mode. Therefore, it is deduced that the probe **2a** is a two-photon excited FRET-based ratiometric fluorescent probe for Cu^{2+}. We hope the detailed investigations can provide a theoretical basis, benefiting to synthesize copper-ion-responsive two-photon FRET ratiometric fluorescent bioimaging reagents.

Acknowledgements

This work was supported by the Natural Science Foundation of China (No. 21473071, No. 21173099, 20973078 and 11404041), the Major State Basis Research Development Program (Grant 2013CB 834801), and special funding to basic scientific research projects for Central Colleges.

References

1 D. T. Quang and J. S. Kim, *Chem. Rev.*, 2010, **110**, 6280–6301.
2 E. L. Que, D. W. Domaille and C. J. Chang, *Chem. Rev.*, 2008, **108**, 1517–1549.
3 E. Gaggelli, H. Kozlowski, D. Valensin and G. Valensin, *Chem. Rev.*, 2006, **106**, 1995–2044.
4 D. R. Brown and H. Kozlowski, *Dalton Trans.*, 2004, 1907–1917.
5 D. Guo, Z. P. Dong, C. Luo, W. Y. Zan, S. Q. Yan and X. J. Yao, *RSC Adv.*, 2014, **4**, 5718–5725.
6 H. Kobayashi, M. Ogawa, R. Alford, P. L. Choyke and Y. Urano, *Chem. Rev.*, 2010, **110**, 2620–2640.
7 J. F. Callan, A. P. Silva and D. C. Magri, *Tetrahedron*, 2005, **61**, 8551–8588.
8 A. P. Demchenko, *Introduction to Fluorescence Sensing*, Springer, New York, 2008.
9 M. Taki, S. Iyoshi, A. Ojida, I. Hamachi and Y. Yamamoto, *J. Am. Chem. Soc.*, 2010, **132**, 5938–5939.
10 D. Wang, Y. Shiraishi and T. Hirai, *Chem. Commun.*, 2011, **47**, 2673–2675.
11 N. Boens, V. Leen and W. Dehaen, *Chem. Soc. Rev.*, 2012, **41**, 1130–1172.
12 L. Yuan, W. Y. Lin, B. Chen and Y. N. Xie, *Org. Lett.*, 2012, **14**, 432–435.
13 X. Sun, P. Liu, L. Wu and B. Liu, *Analyst*, 2015, **140**, 6742–6747.
14 Y. R. Bhorge, T.-L. Chou, Y.-Z. Chen and Y.-P. Yen, *Sens. Actuators, B*, 2015, **220**, 1139–1144.
15 J. Y. Shao, H. Y. Sun, H. M. Guo, S. M. Ji, J. Z. Zhao, W. T. Wu, X. L. Yuan, C. L. Zhang and T. D. James, *Chem. Sci.*, 2012, **3**, 1049–1061.
16 J. L. Fan, M. M. Hu, P. Zhan and X. J. Peng, *Chem. Soc. Rev.*, 2013, **42**, 29–43.
17 A. P. Demchenko, *J. Fluoresc.*, 2010, **20**, 1099–1128.
18 T. Förster, *Ann. Phys.*, 1948, **437**, 55–75.
19 L. Yuan, W. Y. Lin, K. B. Zheng and S. S. Zhu, *Acc. Chem. Res.*, 2013, **46**, 1462–1473.
20 D. L. Graham, P. N. Lowe and P. A. Chalk, *Anal. Biochem.*, 2001, **296**, 208–217.
21 B. Oswald, F. Lehmann, L. Simon, E. Terpetschnig and O. S. Wolfbeis, *Anal. Biochem.*, 2000, **280**, 272–277.
22 J. A. Schmid, P. Scholze, O. Kudlacek, M. Freissmuth, E. A. Singer and H. H. Sitte, *J. Biol. Chem.*, 2001, **276**, 3805–3810.
23 D. M. Willard, L. L. Carillo, J. Jung and A. V. Orden, *Nano Lett.*, 2001, **1**, 469–474.
24 J. Dyer, S. Jockusch, V. Balsanek, D. Sames and N. J. Turro, *J. Org. Chem.*, 2005, **70**, 2143–2147.
25 J. R. Lakowicz, *Principles of Fluorescence Spectroscopy*, Kluwer Academic, New York, 2nd edn, 1999.
26 T. P. Thomas, M. T. Myaing, J. Y. Ye, K. Candido, A. Kotlyar, J. Beals, P. Cao, B. Keszler, A. K. Patri, T. B. Norris and J. R. Baker Jr, *Biophys. J.*, 2004, **86**, 3959–3965.
27 E. W. Miller, A. E. Albers, A. Pralle, E. Y. Isacoff and C. J. Chang, *J. Am. Chem. Soc.*, 2005, **127**, 16652–16659.
28 S. Huang, L.-Y. Zou, A.-M. Ren, J.-F. Guo, X.-T. Liu, J.-K. Feng and B.-Z. Yang, *Inorg. Chem.*, 2013, **52**, 5702–5713.
29 Z. Xu, A.-M. Ren, D. Wang, J.-F. Guo, J.-K. Feng and X. Q. Yu, *J. Photochem. Photobiol., A*, 2014, **293**, 50–56.
30 D. Wang, J.-F. Guo, A.-M. Ren, S. Huang, L. Zhang and J.-K. Feng, *J. Phys. Chem. B*, 2014, **118**, 10101–10110.
31 Y. Chen and A. Periasamy, *Microsc. Res. Tech.*, 2004, **63**, 72–80.
32 J. D. Mills, J. R. Stone, D. G. Rubin, D. E. Melon, D. O. Okonkwo, A. Periasamy and G. A. Helm, *J. Biomed. Opt.*, 2003, **8**, 347–356.
33 L. Z. Liu, G. H. Wei, Z. H. Liu, Z. K. He, S. Xiao and Q. Q. Wang, *Bioconjugate Chem.*, 2008, **19**, 574–579.
34 G. Sivaraman, V. Sathiyaraja and D. Chellappa, *J. Lumin.*, 2014, **145**, 480–485.
35 G. Sivaraman, B. Vidya and D. Chellappa, *RSC Adv.*, 2014, **4**, 30828–30831.
36 M. Beija, C. A. M. Afonso and J. M. G. Martinho, *Chem. Soc. Rev.*, 2009, **38**, 2410–2433.
37 M. L. Bender and B. W. Turnquist, *J. Am. Chem. Soc.*, 1957, **79**, 1889–1893.
38 S. P. Wathen and A. W. Czarnik, *J. Org. Chem.*, 1992, **57**, 6129–6133.
39 V. Dujols, F. Ford and A. W. Czarnik, *J. Am. Chem. Soc.*, 1997, **119**, 7386–7387.

40 H. M. Kim, B. H. Jeong, J. Y. Hyon, M. J. An, M. S. Seo, J. H. Hong, K. J. Lee, C. H. Kim, T. Joo, S. C. Hong and B. R. Cho, *J. Am. Chem. Soc.*, 2008, **130**, 4246–4247.
41 L. Y. Zhou, X. B. Zhang, Q. Q. Wang, Y. F. Lv, G. J. Mao, A. L. Luo, Y. X. Wu, Y. Wu, J. Zhang and W. L. Tan, *J. Am. Chem. Soc.*, 2014, **136**, 9838–9841.
42 Y. Zhao and D. G. Truhlar, *Theor. Chem. Acc.*, 2008, **120**, 215–241.
43 V. M. Aleksandr, J. C. Christopher and G. T. Donald, *J. Phys. Chem. B*, 2009, **113**, 6378–6396.
44 M. J. Frisch, G. W. Trucks, H. B. Schlegel, G. E. Scuseria, M. A. Robb, J. R. Cheeseman, G. Scalmani, V. Barone, B. Mennucci and G. A. Petersson, *et al.*, *Gaussian 09, revisions A.02 and B.01*, Gaussian, Inc., Wallingford, CT, 2009.
45 T. Helgaker, C. Angeli, K. L. Bak, V. Bakken, G. Bin, O. Christiansen, R. Cimiraglia, S. Coriani, P. Dahle and E. K. Dalskov, *et al.*, *Dalton, a molecular electronic structure program*, Release Dalton2011, 2011, see http://daltonprogram.org/.
46 P. R. Monson and W. M. McClain, *J. Chem. Phys.*, 1970, **53**, 29–37.
47 M. Albota, D. Beljonne, J. L. Brédas, J. E. Ehrlich, J.-Y. Fu, A. A. Heikal, S. E. Hess, T. Kogej, M. D. Levin, S. R. Marder, D. McCord-Maughon, J. W. Perry, H. Röckel, M. Rumi, G. Subramaniam, W. W. Webb, X.-L. Wu and C. Xu, *Science*, 1998, **281**, 1653–1656.
48 Y. Liu, Y. Sun, J. Du, X. Lv, Y. Zhao, M. Chen, P. Wang and W. Guo, *Org. Biomol. Chem.*, 2011, **9**, 432–437.
49 H. J. Kim, J. H. Han, M. K. Kim, C. S. Lim, H. M. Kim and B. R. Cho, *Angew. Chem., Int. Ed.*, 2010, **49**, 6786–6789.
50 V. Hrobáriková, P. Hrobárik, P. Gajdoš, I. Fitilis, M. Fakis, P. Persephonis and P. Zahradník, *J. Org. Chem.*, 2010, **75**, 3053–3068.
51 L. T. Bergendahl and M. J. Paterson, *J. Phys. Chem. B*, 2012, **116**, 11818–11828.